

Magnetic properties of commensurate Bose-Bose mixtures in one-dimensional optical lattices

M. Dalmonte^{1,2}, E. Ercolessi¹, M. Mattioli¹, F. Ortolani¹ and D. Vodola¹

¹Dipartimento di Fisica dell'Università di Bologna and INFN, via Irnerio 46, 40126 Bologna, Italy,

²Institute for Quantum Optics and Quantum Information of the Austrian Academy of Sciences, A-6020 Innsbruck, Austria

Abstract. We investigate magnetic properties of strongly interacting bosonic mixtures confined in one dimensional geometries, focusing on recently realized ^{87}Rb - ^{41}K gases with tunable interspecies interactions. By combining analytical perturbation theory results with density-matrix-renormalization group calculations, we provide quantitative estimates of the ground state phase diagram as a function of the relevant microscopic quantities, identifying the more favorable experimental regimes in order to access the various magnetic phases. Finally, we qualitatively discuss the observability of such phases in realistic setups when finite temperature effects have to be considered.

1 Introduction

Experimental advances in the preparation and manipulation of cold atoms and molecules trapped in optical lattices [1, 2] have revived the theoretical interest towards models and problems that in the past played a fundamental role for the description of possible new states of matter, but lacked physical realization in solid state setups. Indeed, thanks to the possibility of using both fermionic and bosonic type of atoms and to the high tunability of the interaction shape and parameters, the phenomena that one can access with these systems are the most varied, ranging from standard superfluidity to BEC-BCS cross-over, to Mott physics and dynamical processes [2–5].

Among the various advantages in dealing with cold atoms, it is worth mentioning the possibility of trapping them in highly anisotropic optical lattices, thus realizing systems with different geometries and dimensions. In particular, strongly anisotropic lattices allow to realize systems in which the atoms are forced to live in one-dimensional (1D) lattices, i.e. on a chain [2, 6].

From a theoretical point of view, physics in 1D is of particular interest not only because it may realize toy models for higher dimensional problems, but also because some physical effects, such as quantum ones, are much stronger and give rise to new phenomena and new states of matter [7, 8]. Analytically, one can use powerful low-energy field theories to describe fermionic, bosonic, and spin models in terms of

collective bosonic degrees of freedom [7, 8]. Also, under suitable hypothesis, one can establish an equivalence between fermionic and spin degrees of freedom.

Theoreticians have long been studying models by switching from a bosonic to a fermionic representation, from a fermion to a spin one, or viceversa. These mappings allow to see how new phases of matter may stabilize for certain values of the coefficients appearing in the Hamiltonian. This is the case, for example, of the emergence of magnetic ordered phases in fermionic and in bosonic models, a problem that was studied long ago in the seminal work by Mott. It was first demonstrated that an insulating antiferromagnetic phase may arise in an apparently simple fermionic model such as the Hubbard one (see [9, 10] for reviews). The analysis has then been extended to more complicated systems, such as mixtures of fermionic species described by the two-species Hubbard model, where also more exotic phenomena may appear (singlet superconductivity, FFLO phase, super-counter-flow, etc.) (see Refs. [2, 6, 11] for a complete review).

As for the bosonic case, it was first in Refs. [12, 13] that it was shown that the Bose-Hubbard model could admit a quantum phase transition from superfluid to an insulating magnetic Mott-like phase. Since then, much attention has been devoted to understand the features of this transition in arbitrary dimensions or in more complex models describing for example mixtures of bosonic species [14–24].

In recent years, these theoretical predictions have become accessible to experimental checks in cold atoms experiments. Starting from the breakthrough demonstration of Mott-insulator to superfluid transition in a gas of Rb atoms [25], strongly correlated regimes have been systematically accessed in ultracold gas experiments, prominent examples being the realization of Tonks-Girardeau [26, 27] and super-Tonks gases [28], the observation of 1D Mott [29] and Berezinskii-Kosterlitz-Thouless transitions [30], and various dynamical processes [2, 31].

Even more intriguing is the possibility of investigating magnetism in such controllable setups, as recently shown in the case of the Ising model in Ref. [32]. In particular, two-species bosonic and fermionic gases represent ideal setups for the search of strongly correlated magnetic states of matter, since once the charge degrees of freedom are gapped in a Mott insulating region, the many-body dynamics is dominated by pseudo-spin degrees of freedom [14, 15, 17], as in the case of the aforementioned Hubbard model [10].

In this work, motivated by impressive experimental achievements in tuning and controlling low-dimensional heteronuclear bosonic mixtures [33, 34], we present a systematic and quantitative investigation for the realization of magnetic phases in a feasible setup of a Bose-Bose mixture of cold atoms trapped in one-dimensional optical lattices. In Sec. 2, we will describe how to model the system via a two-species Bose-Hubbard Hamiltonian, whose effective parameters are determined by microscopic properties, such as the depth of the lattice potential and the Feshbach resonance scattering length. We will discuss this relationship in details for Rb-K mixtures which, thanks to their high tunability [33], allow to span a wide range for both the hopping and the interaction coefficients.

In Sect. 3, we will discuss the theoretical background to study the emergence of magnetic phases in such a system. To describe the physics deep inside the insulating Mott regions, where the single site density is fixed to integer values, we will study the two species Bose-Hubbard Hamiltonian in the strong coupling regime via a perturbative scheme which is a generalization of the Schrieffer-Wolff transformation [35]. At integer fillings, the so obtained effective Hamiltonian can then be mapped onto a spin model, which turns out to be the spin-1/2 XXZ -chain for filling one particle per site and the $\lambda - D$ spin-1 Hamiltonian for filling two. Both these models are paradigmatic for the description of many body systems that display quantum phase transitions [8, 37, 38]. As it is well known, for strong anisotropies, the former one

admits a ferromagnetic and an antiferromagnetic regime. The latter has a very interesting zero-temperature phase diagram, with different critical and massive phases, which include ferromagnetic, Ising-like as well as spin-0 ground states. In particular, it displays a Haldane phase, which is determined by the breaking of a non-local symmetry and described by non-local order parameters, the so-called string-order ones. In both cases, we will address how feasible is to reach these regimes from an experimental point of view.

In Sec. 4, we will study the Bose-Hubbard Hamiltonian in the spin-1/2 magnetic sector by means of numerical simulations based on the density-matrix-renormalization-group (DMRG) algorithm [39, 40]. Our calculations allow to determine a quantitative phase diagram for the experimentally relevant case of Rb-K mixtures. On the basis of this analysis, we will be able to predict the emergence of the various massive phases as the parameters change in an experimentally feasible range, and estimate the critical temperatures needed to achieve such phases in experiments.

Finally, in Sec. 5, we draw our conclusions and discuss possible developments.

2 Model Hamiltonian and experimental regimes

Two-species Bose mixtures strongly confined by optical lattice potentials in two-directions and subject to an additional periodic potential along the third direction are well described by the following microscopic Hamiltonian:

$$\begin{aligned}
 H = & \int dx \sum_{\alpha=1,2} \psi_{\alpha}^{\dagger}(x) \left[-\frac{\hbar^2 \partial_x^2}{2m_{\alpha}} + V(x) + \mu_{\alpha}(x) \right] \psi_{\alpha}(x) + \\
 & + \int dx dx' \sum_{\alpha} \rho_{\alpha}(x) \rho_{\alpha}(x') \mathcal{U}_{\alpha} \delta(x - x') + \\
 & + \int dx dx' \rho_1(x) \rho_2(x') \mathcal{U}_{12} \delta(x - x')
 \end{aligned} \tag{1}$$

Here, $\psi_{\alpha}^{\dagger}, \psi_{\alpha}$ are bosonic creation/annihilation operators, m_{α} are particle masses, $V(x) = V \sin^2(2\pi x/\lambda)$ is the optical lattice potential along the wire of depth V and wavelength λ , and $\mu(x)$ the confining potential along the x -direction. The intra-species interaction strengths $\mathcal{U}_{\alpha} = 2\hbar\omega_{\perp,\alpha} a_{1D,\alpha}$ are related to the intraspecies 1D scattering length $a_{1D,\alpha}$, with $\omega_{\perp,\alpha} = \frac{\hbar\pi}{2m_{\alpha}d^2} \sqrt{V_{\perp}/E_{r,\alpha}}$ being the transverse confinement frequency depending on both the optical lattice spacing $d = \lambda/2$ and the intensity of the transverse field V_{\perp} in units of the recoil energy $E_{r,\alpha} = \frac{\hbar^2}{8m_{\alpha}d^2}$. Finally, the inter-species interaction \mathcal{U}_{12} is usually tunable via Feshbach resonances [41], and is proportional to the inter-species scattering length $a_{1D,12}$. In the limit of sufficiently deep lattice potentials along the wire direction, $V/E_{r,\sigma} \gtrsim 6$, the system is well modeled by an effective Bose Hubbard Hamiltonian:

$$\begin{aligned}
 H_{BB} = & - \sum_{\sigma} t_{\sigma} \sum_i (a_{i,\sigma}^{\dagger} a_{i+1,\sigma} + \text{h.c.}) + U_{ab} \sum_i n_{i,a} n_{i,b} \\
 & + \sum_{\sigma} \frac{U_{\sigma}}{2} \sum_i n_{i,\sigma} (n_{i,\sigma} - 1) + \sum_{\sigma} \mu_{\sigma} \sum_i n_{i,\sigma} (i - L/2)^2
 \end{aligned}$$

where the first term represents tunneling processes of both species $\sigma = 1, 2$, the second and third are the inter- and intra-species interaction, and the last one is a species-dependent confining potential. The operators $a_{j,\sigma}^{\dagger}, a_{j,\sigma}$ satisfy bosonic commutation

relations, and $n_{i,\sigma} = a_{i,\sigma}^\dagger a_{i,\sigma}$. The effective Hubbard parameters can be derived from microscopic quantities by expanding the single particle wave-functions in the Wannier basis, thus obtaining the following relations [2]:

$$t_\sigma = \frac{4E_{r,\sigma}}{\sqrt{\pi}} \left(\frac{V}{E_{r,\sigma}} \right)^{3/4} \exp \left[-2 \left(\frac{V}{E_{r,\sigma}} \right)^{1/2} \right] \quad (2)$$

$$U_\sigma = \frac{\sqrt{2\pi}\mathcal{U}_\sigma}{\lambda} \left(\frac{V}{E_{r,\sigma}} \right)^{1/4} \quad (3)$$

Once a specific experimental setup is considered, the relevant Hamiltonian parameters can be directly shaped by means of external fields as follows: the hopping rate ratio is tuned by considering, e.g., species dependent lattices, or, in case of species independent one, by just changing the lattice depth (which affects more drastically heavier particles). Interactions can be then tuned by Feshbach resonances; in particular, leaving intra-species interactions unmodified, it is possible to span a broad range of interaction strengths by means of an external magnetic field, or, eventually, employing confinement induced resonances.

2.1 Experimental parameters for Rb-K mixtures

As a case study, we will focus from here onwards on ^{87}Rb - ^{41}K mixtures. This choice is justified, from the one hand, by the notable experimental achievements already demonstrated with these mixtures such as, e.g., full tunability of interactions [33], and, on the other hand, by the relative large mass-imbalance, which allows to span parameters regimes ranging from intermediate to large hopping ratios. Here, we consider optical lattices with wavelength $\lambda/2 = 532\text{nm}$ (as reported in [33]), and define dimensionless optical lattice depths $s = V/E_{r,K}$ and $s_\perp = V_\perp/E_{r,K}$ along the x and $y-z$ directions respectively.

Typical experimental parameters obtained from Eq. 2, 3 are presented in Fig. 1. The tunneling rates are strongly suppressed as a function of s , as expected, and in general $U_{Rb} > U_K$. Moreover, in the lower panel, it is shown how inter particle interactions can be increased by considering stronger confinement along $y-z$ directions. The regimes we will be mainly interested in, that is, the ones where magnetic properties may emerge, have to be characterized by sufficiently strong intra-species interactions and not too small hopping rates, so that robustness with respect to temperature is stronger. As such, intermediate values of $s \simeq 10 - 25$ and possibly large values of s_\perp will be our focus from here on.

3 Perturbation theory at integer filling

In this section, we analyse the magnetic phases deep inside the Mott regions at integer filling, $n_{Rb} + n_K \in \mathbb{N}$, $n_K = n_{Rb}$, and discuss the qualitative phase diagrams realistically achievable with Rb-K mixtures. Our treatment flows along the lines of Ref. [15], where the possible magnetic phases of ultra cold atomic mixtures have also been discussed.

In the strong coupling limit ($t_1, t_2 \ll U_{RbK}$, U_1, U_2 , where we have defined 1=K, 2=Rb for compactness), processes in which single particle tunneling changes the total on-site populations require high energy and thus the low energy Hilbert subspace Λ contains only states with a fixed integer occupation number on every site. To derive an

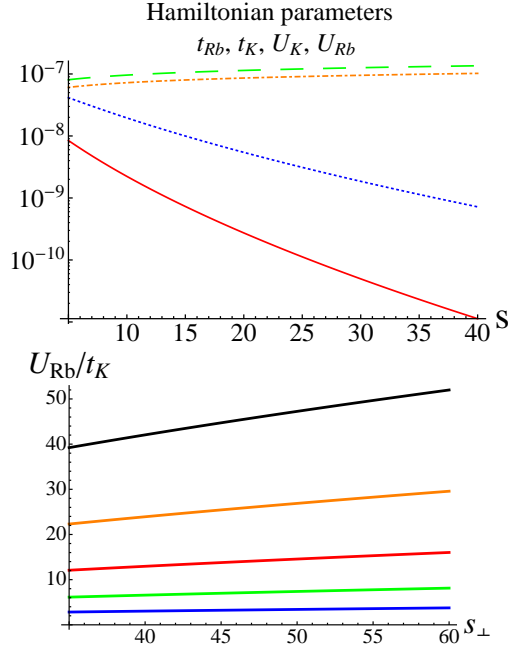


Fig. 1. Typical Hubbard parameters for ^{87}Rb - ^{41}K mixtures. Upper panel: Strength of the different Hamiltonian parameters in K units as a function of the lattice depth along the wire: t_{Rb} (thin, red), t_K (blue, dotted), U_K (dot-dashed, orange), and U_{Rb} (dashed, green). The tunneling rates decrease exponentially when increasing s . Lower panel: intra-species interaction scaling a function of the orthogonal lattice depth s_{\perp} for different values of $s = 10, 15, 20, 25$ from bottom to top.

effective Hamiltonian acting in such subspace we use a generalization of the Schrieffer-Wolff transformation [35, 36].

This kind of technique may be used whenever one has to deal with a Hamiltonian of the type: $H = H_0 + V$, where the unperturbed Hamiltonian H_0 may be diagonalized within a Hilbert subspace Λ [9]. In our case, V contains the hopping terms, whereas two-body interactions determine H_0 . Here, Λ is the subspace with fixed occupation number for every site $n_i \equiv \nu$. By denoting with P, P^{\perp} the orthogonal projectors on the subspaces Λ, Λ^{\perp} respectively, one may write the Hamiltonian as the sum of a diagonal and an off-diagonal term: $H = \mathcal{H}_0 + \mathcal{H}_1$ with

$$\mathcal{H}_0 = PH_0P + P^{\perp}H_0P^{\perp} \quad (4)$$

$$\mathcal{H}_1 = PVP^{\perp} + P^{\perp}VP + P^{\perp}VP^{\perp}. \quad (5)$$

Then one looks for a unitary transformation $U = \exp(i\epsilon S)$, with $S^{\dagger} = S$, that diagonalizes the total Hamiltonian. The operator S may be found by imposing $[\mathcal{H}_0, S] + i\mathcal{H}_1 = 0$, meaning that, up to the first non-trivial correction in ϵ , the diagonal form of H is finally given by:

$$H_{\text{eff}} = \mathcal{H}_0 + i[S, \mathcal{H}_1]. \quad (6)$$

3.1 Spin-1/2 chains for $\nu = 1$

Deep inside the first Mott lobe, when $\nu = 1$, the Hilbert subspace Λ is the tensor product of single-site Hilbert spaces which are two-dimensional and generated by the

two states:

$$|\uparrow_i\rangle \equiv a_{i,1}^\dagger |\text{vac}\rangle, \quad |\downarrow_i\rangle \equiv a_{i,2}^\dagger |\text{vac}\rangle. \quad (7)$$

On this space one can define the spin-1/2 operators:

$$S_i^x = (|\uparrow_i\rangle\langle\downarrow_i| + |\downarrow_i\rangle\langle\uparrow_i|) / 2 \quad (8)$$

$$S_i^y = (|\uparrow_i\rangle\langle\downarrow_i| - |\downarrow_i\rangle\langle\uparrow_i|) / 2i \quad (9)$$

$$S_i^z = (|\uparrow_i\rangle\langle\uparrow_i| - |\downarrow_i\rangle\langle\downarrow_i|) / 2 \quad (10)$$

which allow to rewrite the Schrieffer-Wolff transformed Hamiltonian as:

$$H = \sum_i [J_z S_i^z S_{i+1}^z - J_\perp (S_i^x S_{i+1}^x + S_i^y S_{i+1}^y) - h (S_i^z + S_{i+1}^z) - \lambda \mathbb{I}] \quad (11)$$

where

$$J_z = 2 \frac{t_1^2 + t_2^2}{U_{RbK}} - \frac{4t_1^2}{U_1} - \frac{4t_2^2}{U_2}, \quad J_\perp = \frac{4t_1 t_2}{U_{RbK}}, \quad (12)$$

$$h = \frac{2t_1^2}{U_1} - \frac{2t_2^2}{U_2}, \quad \lambda = \frac{t_1^2}{U_1} + \frac{t_2^2}{U_2} + \frac{t_1^2 + t_2^2}{2U_{RbK}}. \quad (13)$$

Since in any canonical ensemble, h is effectively fixed to 0 (the effects of the trapping potential will be discussed below), we see that, up to a constant factor, the Hamiltonian represents a one-dimensional spin-1/2 XXZ model, as first found in [15]. Interestingly, this basic model displays already a rich phase diagram, characterized by phase transitions from a critical region for $-1 \leq \Delta \equiv J_z/J_\perp \leq 1$ to massive phases, either ferromagnetic (FP) for $\Delta < -1$ or anti-ferromagnetic (AFP) for $\Delta > 1$. In the bosonic language, the former is a super-counter-flow (SCF) superfluid phase, which can be interpreted as a superfluid of particle-hole bound states, as easily seen by performing a particle-hole transformation in one of the species [14].

As shown in Fig. 2, the entire phase diagram can be scanned by just changing the interspecies interaction via Feshbach resonances. For very large values of U_{RbK} , the system displays ferromagnetic behavior, corresponding in the atomic language to real-space phase separation; on the other hand, weak repulsion will indeed favor short-range antiferromagnetic interactions, due to the positive value of the diagonal interaction J_z , as can be noticed from Eq. (13).

3.2 Spin-1 chains for $\nu = 2$ and the Haldane phase

In this section, we analyse the magnetic phases deep inside the Mott region with $\nu = 2$. In this case the low-energy Hilbert subspace is the tensor product of single-site Hilbert spaces which are generated by three states:

$$\begin{aligned} |-1_i\rangle &= \frac{(a_{i,1}^\dagger)^2}{\sqrt{2}} |\text{vac}\rangle, \quad | +1_i\rangle = \frac{(a_{i,2}^\dagger)^2}{\sqrt{2}} |\text{vac}\rangle, \\ |0_i\rangle &= a_{i,1}^\dagger a_{i,2}^\dagger |\text{vac}\rangle \end{aligned} \quad (14)$$

which represent a multiplet for the spin-1 operators [15]:

$$S_i^+ = \sqrt{2} (|+1_i\rangle\langle 0_i| + |0_i\rangle\langle -1_i|) \quad (15)$$

$$S_i^- = \sqrt{2} (|-1_i\rangle\langle 0_i| + |0_i\rangle\langle +1_i|) \quad (16)$$

$$S_i^z = |+1_i\rangle\langle +1_i| - |-1_i\rangle\langle -1_i| \quad (17)$$

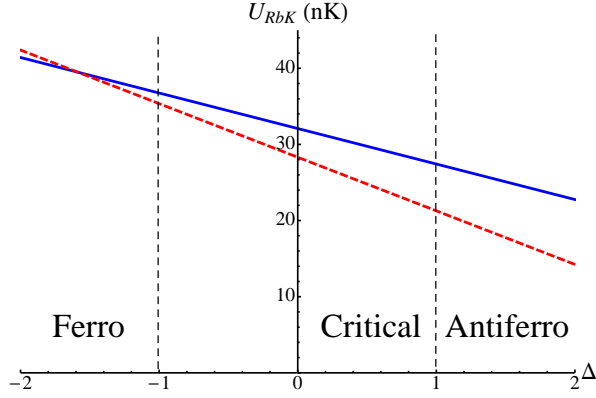


Fig. 2. $\nu = 1, S = 1/2$ case. Evolution of $\Delta = J_z/J_\perp$ with respect to the interspecies interaction U_{RbK} for $s = 9, s_\perp = 65$ (red, dashed line) and $s = 15, s_\perp = 65$ (blue, solid line). The system can be driven from a ferromagnetic to a critical and, eventually, to an anti-ferromagnetic phase, by decreasing U_{RbK} .

By means of the Schrieffer-Wolff transformation, one obtains an effective spin-1 Hamiltonian which, neglecting constant and effective magnetic field terms, is given by:

$$\begin{aligned}
 H_{\text{eff}} = & \sum_i \eta (S_i^x S_{i+1}^x + S_i^y S_{i+1}^y) + \lambda S_i^z S_{i+1}^z + D (S_i^z)^2 \\
 & + \delta (S_i^z S_{i+1}^z)^2 + \zeta (S_i^z (S_{i+1}^z)^2 + (S_i^z)^2 S_{i+1}^z) \\
 & + \chi (\Gamma_i^{xz} \Gamma_{i+1}^{xz} + \Gamma_i^{yz} \Gamma_{i+1}^{yz})
 \end{aligned} \tag{18}$$

where $\Gamma_i^{\alpha\beta} = S_i^\alpha S_i^\beta + S_i^\beta S_i^\alpha$. In terms of the original parameters, the couplings are given by:

$$\begin{aligned}
 \eta = & \frac{1}{2} \left(\frac{t_1 t_2}{U_1 - 2U_{RbK}} + \frac{t_1 t_2}{U_2 - 2U_{RbK}} - \frac{t_1 t_2}{U_1} - \frac{t_1 t_2}{U_2} \right) - \frac{2t_1 t_2}{U_{RbK}} \\
 \lambda = & -\frac{3t_1^2}{U_1} - \frac{3t_2^2}{U_2} + \frac{t_1^2}{2U_{RbK} - U_1} + \frac{t_2^2}{2U_{RbK} - U_2} \\
 D = & \frac{U_1 + U_2 - 2U_{RbK}}{2} + \frac{t_1^2}{2} \left(\frac{3}{U_{RbK} - 2U_1} + \frac{8}{U_1} - \frac{5}{U_{RbK}} \right) \\
 & + \frac{t_2^2}{2} \left(\frac{3}{U_{RbK} - 2U_2} + \frac{8}{U_2} - \frac{5}{U_{RbK}} \right) \\
 \delta = & t_1^2 \left(\frac{3}{U_{RbK} - 2U_1} + \frac{1}{U_1 - 2U_{RbK}} - \frac{7}{U_1} + \frac{5}{U_{RbK}} \right) \\
 & + t_2^2 \left(\frac{3}{U_{RbK} - 2U_2} + \frac{1}{U_2 - 2U_{RbK}} - \frac{7}{U_2} + \frac{5}{U_{RbK}} \right) \\
 \zeta = & \frac{t_1^2}{2} \left(-\frac{3}{U_{RbK} - U_1} - \frac{6}{U_1} + \frac{3}{U_{RbK}} \right) \\
 & + \frac{t_2^2}{2} \left(-\frac{3}{U_{RbK} - U_2} + \frac{6}{U_2} - \frac{3}{U_{RbK}} \right) \\
 \chi = & \frac{t_1 t_2}{2U_1} + \frac{t_1 t_2}{2U_2} - \frac{t_1 t_2}{2U_1 - 4U_{RbK}} - \frac{t_1 t_2}{2U_2 - 4U_{RbK}} - \frac{2t_1 t_2}{U_{RbK}}.
 \end{aligned}$$

In Fig. 3, we show how the different parameters (measured in units of $|\eta|$) depend on the interspecies interaction U_{RbK} for different values of s and s_\perp . In a relatively

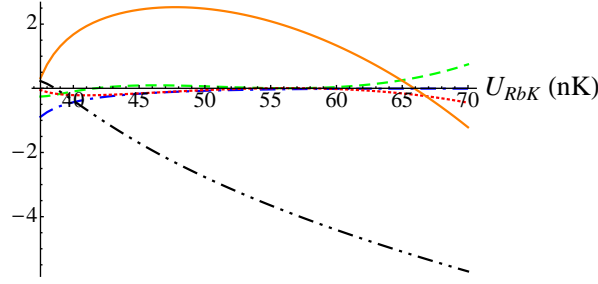


Fig. 3. $\nu = 2, S = 1$ case. The parameters of the effective Hamiltonian (18) as a function of the interspecies interaction U_{RbK} for $s = 9, s_{\perp} = 65$ and assuming $|\eta| = 1$: λ (black, dashed-dotted-dotted), D (orange, solid), δ (green, dashed), ζ (red, dotted) and χ (blue, dashed-dotted). Here, the hopping parameter is $t_K \simeq 22\text{nK}$.

large parameter (U_{RbK}) region, δ, ζ, χ are negligible with respect to λ and D , so the Hamiltonian reduces to that of the so-called $\lambda - D$ model [38, 42]:

$$H_{\lambda-D} = \sum_i \eta(S_i^x S_{i+1}^x + S_i^y S_{i+1}^y) + \lambda S_i^z S_{i+1}^z + D(S_i^z)^2. \quad (19)$$

For example, if $s = 15, s_{\perp} = 65$, this interval is given by $43\text{nK} \lesssim U_{RbK} \lesssim 70\text{nK}$, while if $s = 9, s_{\perp} = 65$ it is given by $36\text{nK} \lesssim U_{RbK} \lesssim 60\text{nK}$.

The ground state phase diagram of the $\lambda - D$ model is even richer than the $S = 1/2$ Heisenberg model one. Some qualitative considerations can be easily made when the first term in eq. (19) can be neglected: if λ is larger than D , the ground state reduces to a ferromagnetic state (if $\lambda < 0$) or antiferromagnetic state (if $\lambda > 0$); if $D \gg |\lambda|$ (large- D phase), spins in all sites prefer to have spin zero. For values of $|D|$ which are comparable with $|\lambda|$, instead, the first term in eq. (19) is important and new phases emerge, as shown numerically in [37], separated by critical lines with different universality classes [43]. More specifically, if λ is negative, the system is critical, belonging to the XX universality class, while for λ positive a new massive phase arises, typical of isotropic spin-1 chain: the Haldane phase [44].

To characterize all massive phases, one may exploit the symmetries of the Hamiltonian. Firstly, it has an explicit Z_2 -symmetry to describe which one can consider the *ferromagnetic order parameter* and the *Néel order parameter* ($\langle \cdot \rangle$ means expectation value in the ground state):

$$\mathcal{O}_{\text{FM}}^{\alpha} = \lim_{|i-j| \rightarrow \infty} \langle S_i^{\alpha} S_j^{\alpha} \rangle; \quad (20)$$

$$\mathcal{O}_{\text{Néel}}^{\alpha} = \lim_{|i-j| \rightarrow \infty} \langle (-1)^{|i-j|} S_i^{\alpha} S_j^{\alpha} \rangle. \quad (21)$$

As shown in [38], the $\lambda - D$ -Hamiltonian has also a hidden $Z_2 \otimes Z_2$ -symmetry which corresponds to a set of non-local order parameters, the so called *string order parameters* [45]:

$$\mathcal{O}_{\text{string}}^{\alpha} = \lim_{|i-j| \rightarrow \infty} \langle -S_i^{\alpha} e^{i\pi \sum_{l=i+1}^{j-1} S_l^{\alpha}} S_j^{\alpha} \rangle, \quad (22)$$

where $\alpha = x, y, z$. The magnetic phase diagram can then be schematically represented as follows: *i*) in the ferromagnetic phase, only $\mathcal{O}_{\text{FM}}^z$ is non zero, while all the other parameters are zero; *ii*) in the Néel phase, $\mathcal{O}_{\text{string}}^{\alpha} = \mathcal{O}_{\text{Néel}}^{\alpha} = 0$ for $\alpha = x, y$, $\mathcal{O}_{\text{FM}}^{\beta} = 0$ for all β , while $\mathcal{O}_{\text{string}}^z$ and $\mathcal{O}_{\text{Néel}}^z$ are non zero; *iii*) in the large- D phase, all the order parameters are zero. Finally, *iv*) in the Haldane phase, all three of $\mathcal{O}_{\text{string}}^{\alpha}$ are non

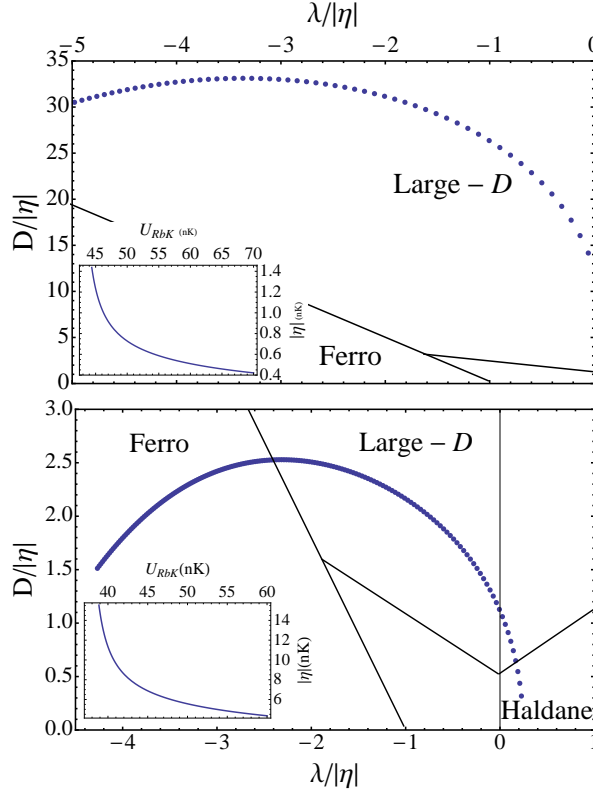


Fig. 4. Phase diagram of Hamiltonian (19) for $s = 15, s_{\perp} = 65$ (upper) and $s = 9, s_{\perp} = 65$ (lower panel). The dots represent the ground state of (19) by varying the interspecies interaction U_{RbK} ($43\text{nK} < U_{RbK} < 70\text{nK}$, lower $38\text{nK} < U_{RbK} < 60\text{nK}$). When U_{RbK} increases the ratio $\lambda/|\eta|$ becomes more negative in both cases. In both insets the parameter η , fixing the energy scale, is plotted versus U_{RbK} .

zero, while all of $\mathcal{O}_{\text{Néel}}^{\alpha}$ and of $\mathcal{O}_{\text{FM}}^{\alpha}$ are zero, so that this phase can be seen as a dilute antiferromagnet, where antiferromagnetic correlations survive despite loosing the associated positional order present in the Néel phase.

From the formulas given above, one can estimate the values of λ and D and thus find that systems with s large ($s \geq 15$) will be mainly in the large- D phase, as it is shown in Fig. 4 (upper panel) for the case with $s = 15, s_{\perp} = 65$ and U_{RbK} in the interval $\sim 43/70\text{nK}$. When the value of s decreases, it is possible to go beyond the large- D phase and, in principle, reach the Haldane phase, as one can see from Fig. 4 (lower panel) for $s = 9, s_{\perp} = 65$ and in a small interval of U_{RbK} .

Nevertheless, we notice that the range of U_{RbK} in which the model reduces to the $\lambda - D$ one is not wide. Also, the Haldane phase region can be reached only for small values of s , where other terms in the effective Hamiltonian may compete with λ, D and affect (or even destroy) topological order. Clearly, both these constraints represent a serious challenge for experimental realizations of the Haldane phase, as a clear observation would require both fine tuning of the parameters and very low temperatures. Finally, since the optical lattice depth in these cases would be of order $s \simeq 9$, it would be preferable to check second order perturbation theory results against more accurate methods such as DMRG or Quantum Monte Carlo simulations.

Phase	Δ_C	Δ_S
AFM	$\neq 0$	$\neq 0$
SCF	$\neq 0$	0
SF _a + SF _b	0	0

Table 1. Strong coupling phases and relation with the charge and spin gaps.

4 Numerical results

In order to complement perturbation theory predictions, we will present here numerical results for the realistic Hubbard parameters discussed in Sec. 2 and equal filling for both species $n_{Rb} = n_K = 1/2$.

Here, we are interested in *i*) determine a quantitative phase diagram spanning a broad range of interaction parameters, and *ii*) determine the optimal parameter regime in terms of resilience to thermal fluctuations, that is, identify the interaction strength around which the smallest between the charge and spin gaps, Δ_c, Δ_s is larger in absolute (that is, when expressed in nK units) value. This last observation is particularly interesting in view of possible experimental investigations, as it provides a quantitative guide to understand the critical temperatures needed to observe magnetic phases. Moreover, such information is not accessible within perturbation theory, as the largest gap region usually lies outside of its applicability regime, as shown below.

All simulations have been carried employing the DMRG algorithm, a state-of-the-art method to tackle ground state properties of 1D systems. In order to determine the quantitative phase diagram of the system and, at the same time, provide relevant energy scales for both charge and spin degrees of freedom, we have investigated the behavior of the charge:

$$\Delta_c(L) = \frac{1}{2} [E_L(L/2 + 1, L/2 + 1) + E_L(L/2 - 1, L/2 - 1) - 2E_L(L/2, L/2)], \quad (23)$$

and spin

$$\Delta_s(L) = \frac{1}{2} [E_L(L/2 - 1, L/2 + 1) + E_L(L/2 + 1, L/2 - 1) - 2E_L(L/2, L/2)], \quad (24)$$

gap, where $E_L(N_1, N_2)$ is the ground state energy at size L in the particle number sector (N_1, N_2) . Far from the ferromagnetic regime $U_{RbK} > U_{Rb}, U_K$, the extrapolated value of the two gaps $\Delta_\alpha = \lim_{L \rightarrow \infty} \Delta_\alpha(L)$ is sufficient to determine the magnetic phase diagram of the system according to Table 1. In particular, the Néel phase is fully gapped, while the super-counter-flow phase, correspondent to the critical phase of the XXZ model, has a finite Δ_c but gapless spin excitations.

In order to suppress boundary effects, we have employed periodic boundary conditions (PBCs); despite being computationally more requiring and limited to relatively small system sizes (here, up to $L = 32$), they assure much better scaling properties since translational symmetry is not explicitly broken, as reflected in the accurate finite-size scaling procedure (illustrated in Fig. 5). High accuracy in ground state and excited state energies (with discarded weights usually of order 5×10^{-6} or smaller) have been achieved by employing up to 1024 states per block and 5 finite-size sweeps, and further enhanced by applying an iterative procedure which used the final finite-size step at size $L - 2$ as the initial one at size L . Moreover, in each ground state sector, four states were usually targeted. In most simulation, a single-site basis of 8 states (considering Rb particles as hard core) is sufficient to faithfully represent a realistic system; this feature has been systematically verified for small system sizes ($L \leq 12$), and by using a 15 state single-site basis close to critical points.

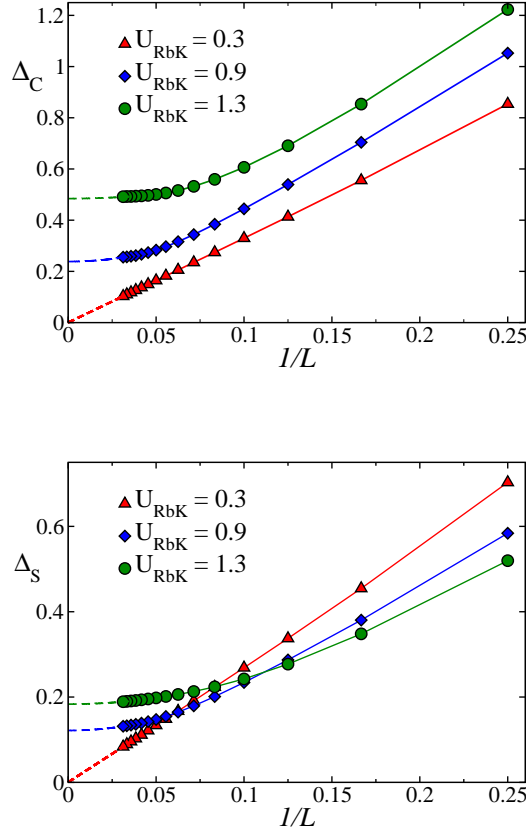


Fig. 5. Finite-size scaling analysis for both charge (upper panel) and spin (lower panel) gaps; here, $s = 26, s_{\perp} = 70$, and inter particle interactions are varied. In both panels, lines are linear ($U_{RbK} = 0.3$) and algebraic (others) best fits.

As a case study, we considered fixed values of the optical lattice depth, and investigate the quantum phase diagram as a function of the inter-species interaction strength. This choice is motivated by the experimentally demonstrated tunability of Rb-K interactions [33], which allows to span large interaction regimes by keeping the same lattice structure. In Table 2, we list the optical lattice setups investigated numerically, together with the corresponding hopping ratio.

As already mentioned, PBCs assure very good scaling properties during the finite size procedure, where we have always considered polynomial scaling of the form:

$$\Delta_{\alpha}(1/L = x) = a_0 + a_1x + a_2x^2. \quad (25)$$

Different scaling *ansätze* with higher order contributions do not lead to significant quantitative changes. Typical results are shown in Fig. 5, illustrating how both gaps opens for relatively small coupling strengths.

For all values listed in Table 2, we observe the expected phase diagram, which, as a function of U_{RbK} , presents a fully gapless phase first, then an antiferromagnetic insulator, which melts into a SCF phase for relatively large values of the interaction

s	20	20	26	26
s_{\perp}	50	80	70	90
t_K (nK)	5.4	5.4	2.8	2.8
t_{Rb}/t_K	0.050	0.050	0.033	0.033

Table 2. Optical lattice configurations investigated in this section, together with correspondent hopping asymmetry and typical energy scales.

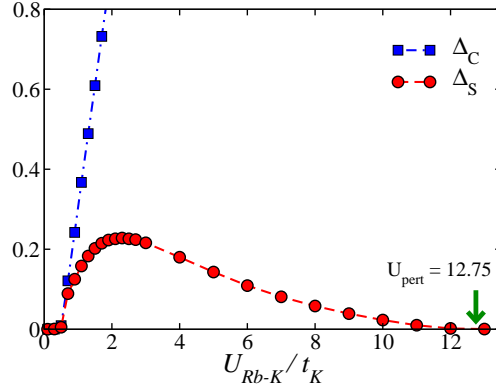


Fig. 6. Charge and spin gaps as a function of the inter particle interaction. While the charge gap increases significantly and then saturates as a function of U_{RbK} , the spin gap displays a non-monotonic behavior; it opens almost simultaneously as Δ_c (making the SCF region at small U very thin), displays a maximum around $U_{RbK} \simeq 2$, and then decreases till the BKT point separating the Néel phase from another SCF region. Numerical results show a good agreement with second order perturbation theory estimate (based on Eq. (12), (13)), indicated by a green arrow.

strength. It is worth noticing that our procedure is not accurate enough to resolve a possible weak coupling SCF phase between fully gapless and AF phases; since the gap is expected to open according to Berezinskii-Kosterlitz-Thouless scaling [7], refined methods should in principle be employed in order to quantitatively tackle this issue. Nonetheless, such SCF phase will occupy a very small parameter region with extremely small charge gap, making its experimental observation extremely challenging.

Close to the SCF-AF critical point, we find excellent agreement between numerical and perturbation theory results, as illustrated in Fig. 6; we can then faithfully estimate the extent of the SCF region at strong coupling by using the results presented in Sec. 3. Depending on the values of s, s_{\perp} , the SCF is present in a region which is relatively wide, of order $U_{RbK}/t_K \simeq 2$, making its strong coupling observation accessible in tunable systems.

A crucial point in the search for magnetic phases in ultra cold atomic systems is the competition between thermal fluctuations and Néel order. At a qualitative level, one expects that larger spin gaps could provide stronger finite-temperature signatures of ground state physics, since thermal fluctuations would then be not sufficiently strong to *activate* spin excitations. In Fig. 7, we plot the spin gap in temperature units (K) for several choices of the lattice configuration as a function of the inter particle interactions.

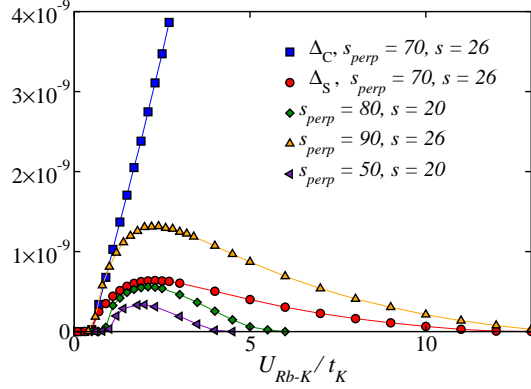


Fig. 7. Charge and spin gaps (expressed in K units) as a function of the inter particle interaction. The maximum value of the spin gap is always reached far from the perturbative regime, making perturbation theory not fully reliable when estimating critical energy scales.

Three main features emerge from the quantitative analysis. The first one is, very deep lattices favor larger values of Δ_s , as expected, since they increase the ratio between intra-species interactions and tunneling rates. Secondly, we observe a quasi-plateau structure of the spin gap, that is, its value is almost constant in a finite region of the AF phase; this implies that inter-species interactions do not need accurate finite tuning in order to find the optimal experimental configuration. Finally, it is worth noticing how the maximal value of Δ_s is usually far from the perturbative limit, signaling how strong coupling perturbation theory is usually not a fully trustable tool in order to identify optimal experimental regimes where to search for AF.

Finally, let us comment on the $\nu = 2$ case. As suggested by the results discussed in the previous section, the topological Haldane phase may emerge, but in very tiny parameter regimes; as such, it'd be interesting to investigate if such regimes, at least in the perturbative limit and eventually via more accurate numerical techniques, may enlarge in presence of larger mass imbalance by considering, e.g., ^6Li - ^{133}Cs mixtures.

5 Discussion and conclusions

We discussed magnetic phases in commensurate bosonic ultracold atomic gases, focusing on the recently realized ^{87}Rb - ^{41}K mixtures in 1D optical lattices. After an analysis on the relation between microscopic and Hubbard parameters, we presented a combined analytical and numerical study on the emergent insulating phases in such systems. By means of perturbation theory, we illustrated the general magnetic scenarios accessible in such setups by comparing effective spin-chain Hamiltonians with the accessible parameter regimes, focusing on the relevant cases of $S = 1/2$ and $S = 1$ spin representations. In the latter case, we showed how, while the so called *large-D* and ferromagnetic phases (phase separation) are well within reach, exploring topological states of matter such as the Haldane phase will represent a notable experimental challenge. In the former, we discussed how the entire strong coupling phase diagram, including ferromagnetic, antiferromagnetic, and super-counter-flow phases, may be experimentally accessed by tuning the interspecies repulsion by means of, e.g., a Feshbach resonance [33]. As a quantitative benchmark for experimental realizations, we

have investigated the phase diagram of these systems by means of DMRG simulations. By evaluating the typical energy gaps in the systems, we estimated the optimal optical lattice setups in order to observe anti-ferromagnetism in cold atomic gases, finding that experimentally challenging but accessible temperatures [34] in the nK range are required to unambiguously reach such regimes.

Acknowledgements

We would like to thank the entire LENS group, and in particular J. Catani, G. Lamporesi, and F. Minardi, for useful discussion on the experimental issues, and C. Degli Esposti Boschi, M. Di Dio and T. Roscilde for discussions on theoretical aspects. M.D. acknowledges support by the European Commission via the integrated project AQUITE. This work was supported in part by INFN COM4 grant NA41.

References

1. D. Jaksch, C. Bruder, J. I. Cirac, C. Gardiner and P. Zoller, Phys. Rev. Lett. **81**, 3108 (1998).
2. I. Bloch, J. Dalibard and W. Zwerger, Rev. Mod. Phys. **80**, (2008) 885.
3. S. Giorgini, L. P. Pitaevskii and S. Stringari, Rev. Mod. Phys. **80**, (2008) 1215.
4. F. Dalfovo, S. Giorgini, L. P. Pitaevskii and S. Stringari, Rev. Mod. Phys. **71**, (1999) 463.
5. M. Lewenstein, A. Sanpera, V. Ahufinger, B. Damski, A. Sen De and Ujjwal Sen, Adv. in Phys. **56**, 1-2 (2007) 243.
6. M. A. Cazalilla, R. Citro, T. Giamarchi, E. Orignac and M. Rigol, Rev. Mod. Phys. **83**, (2011) 1405.
7. A.O. Gogolin, A.A. Nersisyan, A.M. Tsvelik, *Bosonization and strongly correlated systems*, (Cambridge University press, Cambridge, 1998).
8. T. Giamarchi, *Quantum Physics in one dimension*, (Oxford University press, Oxford, 2003).
9. A.P. Balachandran, E. Ercolessi, G. Morandi and A.M. Srivastava, *Hubbard Model and Anyon Superconductivity*, World Scientific, Singapore, 1990.
10. F. Essler, H. Frahm, F. Göhmann, A. Klümper and V. Korepin, *The One-Dimensional Hubbard Model*, Cambridge University Press, Cambridge, 2005.
11. A. Feiguin, F. Heidrich-Meisner, G. Orso, and W. Zwerger, Lect. Not. Phys. **836**, (2011) 503.
12. T. Giamarchi and H. J. Schulz, Phys. Rev. B **37**, (1988) 325.
13. M. Fisher, P.B. Weichman, G. Grinstein and D.S. Fisher, Phys. Rev. B **40**, (1989) 546.
14. A.B. Kuklov and B. Svistunov, Phys. Rev. Lett. **90**, (2003) 100401.
15. E. Altman, W. Hofstetter, E. Demler and M.D. Lukin, New J. Phys. **5**, (2003) 113.
16. B. Capogrosso-Sansone, S.G. Söyler, N. V. Prokof'ev and B.V. Svistunov, Phys. Rev. A **81**, (2010) 053622.
17. M. Guglielmino, V. Penna and B. Capogrosso-Sansone, Phys. Rev. A **82**, (2010) (R) 021601.
18. T. Roscilde, C. Degli Esposti Boschi and M. Dalmonte, EPL **97**, (2012) 23002.
19. A. Hubener, M. Snoek and W. Hofstetter, Phys. Rev. A **80**, (2009) 245109.
20. A. Hu, L. Mathey, I. Danshita, E. Tiesinga, C.J. Williams and C.W. Clark, Phys. Rev. A **80**, (2009) 023619.
21. L. Mathey, Phys. Rev. B **75**, (2007) 144510.
22. M. Dalmonte, K. Dieckmann, T. Roscilde, C. Hartl, A.E. Feiguin, U. Schollwöck and F. Heidrich-Meisner, Phys. Rev. A **85**, (2012) 063608.
23. T. Roscilde and J.I. Cirac, Phys. Rev. Lett. **98**, (2007) 190402.

24. A. Isacsson, Min-Chul Cha, K. Sengupta and S.M. Girvin, *Phys. Rev. B* **72**, (2005) 184507.
25. M. Greiner, O. Mandel, T. Esslinger, T.W. Hänsch and I. Bloch, *Nature* **415**, (2002) 39.
26. B. Paredes, A. Widera, V. Murg, O. Mandel, S. Fölling, I. Cirac, G.V. Shlyapnikov, T.W. Hänsch and I. Bloch, *Nature* **429**, (2004) 277.
27. T. Kinoshita, T. Wenger and D. S. Weiss, *Science* **305**, (2004) 1125.
28. E. Haller, M. Gustavsson, M.J. Mark, J.G. Danzl, R. Hart, G. Pupillo and H.-C. Nägerl, *Science* **325**, (2009) 1224.
29. T. Stöferle, H. Moritz, C. Schori, M. Köhl and T. Esslinger, *Phys. Rev. Lett.* **92**, (2004) 130403.
30. E. Haller, R. Hart, M.J. Mark, J.G. Danzl, L. Reichsöllner, M. Gustavsson, M. Dalmonte, G. Pupillo and H.-C. Nägerl, *Nature* **466**, (2010) 597.
31. T. Kinoshita, T. Wenger and D. S. Weiss, *Nature* **440**, (2006) 900.
32. J. Simon, W.S. Bakr, R. Ma, M.E. Tai, P. M. Preiss and M. Greiner, *Nature* **472**, (2011) 307.
33. G. Thalhammer, G. Barontini, L. De Sarlo, J. Catani, F. Minardi and M. Inguscio, *Phys. Rev. Lett.* **100**, (2008) 210402.
34. J. Catani, G. Barontini, G. Lamporesi, F. Rabatti, G. Thalhammer, F. Minardi, S. Stringari and M. Inguscio, *Phys. Rev. Lett.* **103**, (2009) 140401.
35. J.R. Schrieffer and P.A. Wolff, *Phys. Rev.* **149**, (1966) 491.
36. L. Barbiero, M. Casadei, M. Dalmonte, C. Degli Esposti Boschi, E. Ercolessi and F. Ortolani, *Phys. Rev. B* **81**, (2010) 224512.
37. W. Chen, K. Hida and B. C. Sanctuary, *Phys. Rev. B* **67**, (2003) 104401.
38. T. Kennedy and H. Tasaki, *Commun. Math. Phys.* **147**, (1992) 431.
39. S. R. White, *Phys. Rev. Lett.* **69**, (1992) 2863.
40. U. Schollwöck, *Rev. Mod. Phys.* **77**, (2005) 259.
41. C. Chin, R. Grimm, P. Julienne and E. Tiesinga, *Rev. Mod. Phys.* **82**, (2010) 1225.
42. H.J. Schulz, *Phys. Rev. B* **34**, (1986) 6372.
43. C. Degli Esposti Boschi, E. Ercolessi, F. Ortolani and M. Roncaglia, *Eur. Phys. J. B* **35**, (2003) 465.
44. F.D.M. Haldane, *Phys. Rev. Lett.* **50**, (1983) 1153.
45. M. den Nijs and K. Rommelse, *Phys. Rev. B* **40**, (1989) 4709.